IN-24
61937
P-13

NASA Technical Memorandum 105305

Thermally-Driven Microfracture in High Temperature Metal Matrix Composites

Subodh K. Mital
University of Toledo
Toledo, Ohio

and

Christos C. Chamis
Lewis Research Center
Cleveland, Ohio

Prepared for the
Symposium on the Mechanics of Composites at Elevated and Cryogenic Temperatures, ASME Applied Mechanics and Biomechanics Summer Conference
Columbus, Ohio, June 16–19, 1991

NASA

THERMALLY-DRIVEN MICROFRACTURE IN HIGH TEMPERATURE METAL MATRIX COMPOSITES

Subodh K. Mital*
University of Toledo
Toledo, Ohio 43606

and

Christos C. Chamis
National Aeronautics and Space Administration
Lewis Research Center
Cleveland, Ohio 44135

ABSTRACT

Microfracture (fiber/matrix fracture, interphase debonding and interply delamination) in high temperature metal matrix composites (HTMMC), subjected to thermal loading, is computationally simulated. Both unidirectional and crossply SiC/Ti15 composites are evaluated for microfracture driven by thermal loads, using multicell finite element models. Results indicate that under thermal loads alone, microfracture propagation is not as sensitive as it is under mechanical loads.

INTRODUCTION

High temperature metal matrix composites (HTMMC) are potential structural materials for advanced propulsion systems, demanding high operational temperatures (400 to 1100 °C). High moduli and strength, tailorable properties, dimensional stability and hygral (moisture) resistance make these materials especially attractive for the aerospace industry. Microfracture in HTMMC is critical to assess their structural integrity and durability. Traditionally, researchers looked at the microfracture using stresses, strains and stress intensity factors at the local level for the crack initiation and propagation. Such procedures are complex, computationally intensive and difficult to observe by conventional experiments. An alternate approach is to assess the effect of microfracture on the global response (displacement, work done etc.).

In previous investigations (refs. 1 and 2), microfracture was computationally simulated for unidirectional and crossply metal matrix composites subjected to various types of mechanical loads. Microfracture propagation and the extent of stress redistribution in the surrounding fiber and matrix due to fiber/matrix fracture, interphase debonding and inter-ply delamination, were computationally simulated. A computational simulation procedure based on three-dimensional finite element analysis and global strain energy release rates was developed, to predict the microfracture process and identify/quantify the hierarchy of respective fracture modes under various types of loading. Step-by-step procedures were outlined to evaluate composite microfracture and establish the hierarchy of respective fracture modes for a given composite system. Typical results indicate that if the composite is subjected to longitudinal (along the fiber) loading, interphase debonding is not likely to initiate by itself. It will only occur if it is preceded

*NASA Resident Research Associate at Lewis Research Center.

by fiber or matrix fracture. This demonstrates that debonding is a weaker fracture mode and very likely, it will instantaneously follow the stronger fracture modes (fiber/matrix fracture) when the composite is subjected to longitudinal tensile loads. Typical strain energy release rate curves for a unidirectional SiC/Ti15 0.35 fvr composite subjected to longitudinal load are shown in figure 1. It shows that debonding mode of fracture requires less energy to propagate and occurs following either the fiber or the matrix fracture. Microfracture was also simulated for other types of mechanical loading. Similar observations were made for other types of mechanical loading in both unidirectional and crossply composite laminates.

The objective of the present paper is to outline a procedure to computationally simulate microfracture and identify/quantify the microfracture modes and propagation for unidirectional and crossply metal matrix composite laminates subjected to thermal loads.

FINITE ELEMENT MODEL

The finite element models used in the computational simulation procedure consist of a group of nine fibers in a three-by-three unit cell array ("nine cell model"). The unidirectional composite system consists of 35 percent fiber volume ratio (fvr) SiC/Ti15 metal matrix composite (silicon carbide fiber and titanium alloy matrix). There are 16 nodal segments ("bays") along the length of the fiber. Each unit cell as shown in figure 2, consists of 40 hexahedron (six-sided) and 8 pentahedron (five-sided) solid elements for a total of 6912 elements and 6953 nodes in the model. The crossply composite has three plies with 0/90/0 lay-up, as shown in figure 3, and is a 30 percent fvr SiC/Ti15 metal matrix composite. There are six bays along the length of the fiber in both 0° and 90° plies. Each unit cell consists of 40 hexahedron (six-sided) and 8 pentahedron (five-sided) solid elements for a total of 2592 elements and 2863 nodes in the model. The properties of the constituents at the reference (room) temperature are shown in table I.

In this composite, the coefficient of thermal expansion (CTE) of the matrix is more than that of the fiber ($\alpha_m > \alpha_f$). The matrix longitudinal stress due to the cooldown from processing to use temperature is tensile. The corresponding fiber longitudinal stress is compressive. In the case of the crossply composite, there is also a mismatch between the thermal expansion coefficient of the 0° and 90° plies, resulting in higher matrix microstresses. In any case, the matrix microstresses are tensile, while the fiber microstresses are compressive. Because of this stress state, the fracture is likely to initiate in the matrix. It is then propagated either through the fiber-matrix interface to cause debonding or through the interply layer to cause delamination. In the simulation, fracture is introduced around the fiber, such that the whole fiber circumference is debonded. Fracture is simulated by placing duplicate node points on either side of the crack. These duplicate nodal or grid points have the same geometrical location, but no connectivity exists between them, thus, in effect producing a crack of zero width. Symmetry boundary conditions are applied in the middle planes, so that the composite is free to move on either side when thermal loads are applied. Resulting stresses and internal strain energy corresponding to those applied thermal loads is computed by the finite element analysis. The corresponding strain energy release rates are computed for perturbed fracture configurations by using the definitions described below. Strain energy release rates (SERR) for different fracture modes are then compared to establish the fracture process, identify/quantify the various fracture modes and establish the hierarchy of those fracture modes.

STRAIN ENERGY RELEASE RATE

The strain energy release rate (SERR) is an acceptable indicator of the fracture toughness of a material. It gives a measure of the amount of energy required to propagate a defect in a material. Hence, one can make a direct comparison of damage tolerances between different microfracture configurations (modes/paths), materials and geometries. One of the methods used to calculate SERR is the crack closure method. In this method, nodal displacements and corresponding nodal forces at the crack tip location, are used to determine the amount of work required to close the crack, which has been extended by an incremental amount.

The above approach is a local or microfracture approach since the amount of energy produced by the local displacements and forces at the crack tip location are used to calculate the corresponding strain energy release rates. Another approach to calculate global SERR is to compare internal strain energies of small fracture propagations. The strain energy release rate is then, calculated as:

$$G = \frac{dW}{dA} = \frac{1}{2} \cdot \frac{(S.E.)_2 - (S.E.)_1}{\Delta A} \tag{1}$$

where

dW	incremental work done
ΔA	area of the new surfaces generated
$(S.E.)_1$, $(S.E.)_2$	strain energy prior to and after ΔA, respectively

The SERR were computed by using both the crack closure method and by using global strain energy for one case to compare the values. Both methods give the same results, although using the global strain energy approach is computationally more effective and direct. However, the crack closure method is required to identify each failure mode in the presence of combined mode fracture. The global strain energy approach is used in the present work. The advantage of using the global SERR approach is that it bypasses local stress details to describe stress gradients that usually require relatively fine meshes.

MULTIFACTOR INTERACTION RELATIONSHIP

Constituent material properties are required at higher use temperatures. Constituent material properties at reference (room) temperatures are known, as shown in table I. The effect of temperature on material properties is taken into account by using a multifactor interaction relationship (refs. 3 and 4) as shown in figure 4. It models the material behavior using a time-temperature-stress dependence of the constituent's properties in a "material behavior space," as follows:

$$\frac{P}{P_0} = \left[\frac{T_F - T}{T_F - T_0}\right]^n \cdot \left[\frac{S_F - \sigma}{S_F - \sigma_0}\right]^m \cdots \tag{2}$$

where

P property

T temperature

S strength

σ stress

0 reference

F final

m,n are exponents

It assumes that various factors such as temperature, stress, stress rate, etc. influence the in-situ constituent material behavior. The multifactor interaction relationship (eq. (2)) represents gradual effects during most of the range and rapidly degrading properties near the final stages as has been observed experimentally (ref. 5). The exponents are determined from experimental data, wherever possible, otherwise default values for exponents are used which are based on "best judgment" from studies conducted on other materials (ref. 5).

In the present investigation, in-situ properties are assumed to depend only on temperature ($m = 0$). The value of exponent n is taken as 0.5 for matrix and 0.25 for fiber. The final temperature is assumed to be the melting temperature of the constituent and the reference temperature is taken as the room temperature (21 °C/70 °F). For example, to calculate a matrix property at 815 °C, where the titanium alloy matrix melting point is taken as 927 °C (1700 °F), then from equation (2):

$$\frac{P}{P_0} = \left[\frac{927 - 815}{927 - 21}\right]^{0.5} = 0.35$$

Any matrix property, i.e., modulus, at 815 °C will be 35 percent of the reference property, i.e., room temperature modulus. In the case of α, coefficient of thermal expansion, the exponent n is assumed to be negative, because α is assumed to increase with increase in temperature. Constituent material properties at 815 °C (1500 °F), calculated using equation (2) are shown in table II.

RESULTS/DISCUSSION

In the first set of simulations, both unidirectional and crossply composites were uniformly heated from room temperature (21 °C/70 °F) to a temperature of 300 °C (570 °F), i.e., ΔT of 280 °C (500 °F). Constituent properties at room temperature were used and were assumed to remain constant for this thermal loading case. In the case of the unidirectional composite, fracture was initiated in the matrix at the middle plane of the center cell and then propagated through the fiber-matrix interface. The change in total strain energy was very small. Even when all the fibers were debonded, the change in total strain energy and the corresponding SERR were negligibly small (G = 0.02 lb/in.). In the case of crossply composite, fracture was again initiated in the matrix at the middle plane of the center cell and propagated along the fiber-matrix interface. When the center cell fiber was fully debonded, the change in total strain

energy, from reference (no fracture) state to this fracture mode, was 0.4 percent. The corresponding strain energy release rate was also negligibly small. Fracture initiated at that location was also propagated to the interply layer in order to simulate delamination between the top and middle plies. When the delamination extended up to four bays through the width (y-direction) and in the x-direction, there was no noticeable change in the total strain energy as compared to the reference state. Hence, it can be concluded for both unidirectional and crossply composites, that thermally driven microfracture propagation is quite insensitive to temperature increases up to 260 °C (500 °F) from the reference (room) temperature.

In the next set of simulations, the composites were cooled down from 815 °C (1500 °F) to -185 °C (-300 °F), i.e., a ΔT of -1000 °C (-1800 °F). Constituent material properties were computed at 815 °C (1500 °F), shown in table II, by using equation (2) and were assumed to remain constant through this thermal load. Since, the CTE increases with increase in temperature, the mismatch in CTE of the fiber and the matrix is very high at 815 °C (table II). As mentioned before, the thermal expansion coefficient of the titanium alloy (Ti15) matrix is more than the thermal expansion coefficient of the silicon carbide (SiC) fiber. Thus, during the cool down process from high temperatures to cryogenic temperatures, the fiber develops compressive longitudinal stress, while the matrix is under tensile longitudinal stress. Therefore, the microfracture is likely to initiate in the matrix. In the case of the unidirectional composite, the microfracture was initiated in the middle plane of the center cell matrix and propagated in the matrix or through the fiber-matrix interface. The SERR curve for fracture propagation through the fiber-matrix interface is shown in figure 5. Hence, it can be concluded that once approximately 10 percent of the fiber surface is debonded, debonding can propagate at the same energy level. The SERR for the case when the fracture propagates in the matrix is zero. Thus, the fiber-matrix interface debonding is the only likely mode of fracture propagation in this case. The unidirectional composite, therefore, will exhibit matrix cracking or a significant amount of interface debonding and is unlikely to fail in a brittle manner.

In the case of the crossply composite, cracks can initiate in the 90° ply as intraply cracks or through the thickness of the 90° ply as transply cracks. When the crack initiates within the 90° as an intraply crack at the mid-length of the fiber (fig. 6), it propagates in the matrix and then the fiber-matrix interface to debond the adjacent center cell fiber. The SERR curve as the center cell fiber debonds is shown in figure 6. The curve shows the same pattern as observed earlier, once about 10 percent of the fiber surface is debonded, debonding can propagate at the same energy level. If the crack initiates in the matrix as a transply or through-the-thickness crack at the center of the specimen, then it can propagate through the matrix to debond the fiber in the adjacent (0°) ply, or it can propagate through the interply layer to cause delamination. When the transply crack propagates in the interply layer, there is no change in the global strain energy and thus, the SERR is also zero. However, if the transply crack propagates through the matrix and debonds the adjacent ply fiber, the SERR for that fracture mode is shown in figure 7. As before, the fiber-matrix interface debonding is the only mode of fracture propagation in this composite. Hence, it can be concluded that thermally-driven microfracture in crossply composites will exhibit matrix cracking and fiber debonding due to the cool down from high temperatures to cryogenic temperature and the microfracture will not propagate in the interply layer to cause delamination.

Other thermal loading cases involving thermal gradients were also evaluated, including one in which the top surface was maintained at a very high (815 °C/1500 °F) temperature and bottom surface was maintained at cryogenic (-300 °F/-185 °C) temperature. In other loading case, top and bottom surfaces were maintained at 538 °C/1000 °F and the middle plane was

kept at 815 °C/1500 °F. Both of these cases did not exhibit any sensitivity for microfracture propagation in either unidirectional or crossply composite. The results for microfracture initiation and propagation are summarized in table III. For example, in the case of the unidirectional composite subjected to a uniform temperature increase, the microfracture is likely to initiate in the matrix and propagates through the fiber-matrix interface. If the microfracture initiates in the interphase region or the interply region (pre-existing crack), it does not propagate when subjected to such a thermal load.

CONCLUSIONS

A computational simulation procedure is described for microfracture initiation and propagation in metal matrix composites subjected to thermal loading. The procedure is applied to evaluate microfracture for both unidirectional and crossply composites. The significant results from this investigation are as follows:

1. The crack closure method and the global strain energy methods give the same results for strain energy release rates (SERR). The global strain energy method is computationally more effective. However, crack closure method should be used to identify the individual modes of fracture in cases of mixed mode fracture.

2. In general, microfracture propagation in HTMMC is not as sensitive to thermal loads as it is to mechanical loads.

3. For both unidirectional and crossply composites, microfracture propagation is not sensitive for a temperature increase of 260 °C/500 °F from room temperature.

4. When cooled down from high temperature to cryogenic temperature, the fracture initiates in the matrix:

   i. For unidirectional composites, fiber-matrix interface is the only likely mode of fracture propagation.

   ii. For crossply composites:

      a. If the crack initiates within a ply between the fibers (intraply cracks), it propagates to debond the adjacent fiber.

      b. If the crack initiates through the thickness of the ply (transply crack), it propagates to the adjacent ply and debonds the fiber in that ply.

      c. If the transply crack initiates closer to a fiber, it debonds the adjacent fiber within the ply.

REFERENCES

1. Mital, S.K.; Caruso, J.J.; and Chamis, C.C.: Metal Matrix Composites Microfracture: Computational Simulation. Comput. Struct., vol. 37, no. 2, 1990, pp. 141-150, (also, NASA TM-103153).

2. Mital, S.K.; and Chamis, C.C.: Microfracture in High Temperature Metal Matrix Crossply Laminates. NASA TM-104381, 1991.

3. Hopkins, D.A.; and Chamis, C.C.: A Unique Set of Micromechanics Equations for High Temperature Metal Matrix Composites. NASA TM-87154, 1985.

4. Murthy, P.L.N.; Hopkins, D.A.; and Chamis, C.C.: Metal Matrix Composite Micromechanics: In-Situ Behavior Influence on Composite Properties. NASA TM-102302, 1989.

5. Chamis, C.C., et al.: METCAN Verification Status. NASA TM-103119, 1990.

TABLE I. - PROPERTIES OF CONSTITUENT MATERIALS OF SiC/Ti15 AT ROOM TEMPERATURE

	SiC fiber	Ti15 matrix	Inter-phase
Modulus, E (Mpsi)	62.0	12.3	12.3
Poisson's ratio, ν	.3	.32	.32
Shear modulus, G (Mpsi)	23.8	4.8	4.8
Coefficient of thermal expansion, α, (ppm/°F)	1.8	4.5	4.5

TABLE II. - PROPERTIES OF CONSTITUENT MATERIALS OF SiC/Ti15 AT 815 °C (1500 °F)

	SiC fiber	Ti15 matrix	Inter-phase
Modulus, E (Mpsi)	57.0	4.3	4.3
Poisson's ratio, ν	.28	.15	.15
Shear modulus, G (Mpsi)	22.4	1.9	1.9
Coefficient of thermal expansion, α, (ppm/°F)	1.96	12.8	12.8

TABLE III. - MICROFRACTURE INITIATION AND MODE HIERARCHY UNDER THERMAL LOADS

Composite/Load \ Constituent		Fiber (f)		Matrix (m)		Interphase (i)		Interply layer (ip)	
		I[a]	P[b]	I	P	I	P	I	P
Unidirectional composite (UDC)	Uniform temperature			m		i	m	ip	
	Thermal gradient through-the-thickness			m		i		ip	
Crossply composite (CPC)	Uniform temperature			m		i	m	ip	
	Thermal gradient through-the-thickness			m		i		ip	

[a]I: microfracture initiation.
[b]P: microfracture propagation.

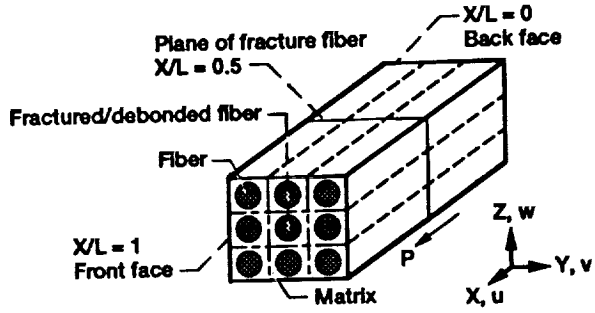

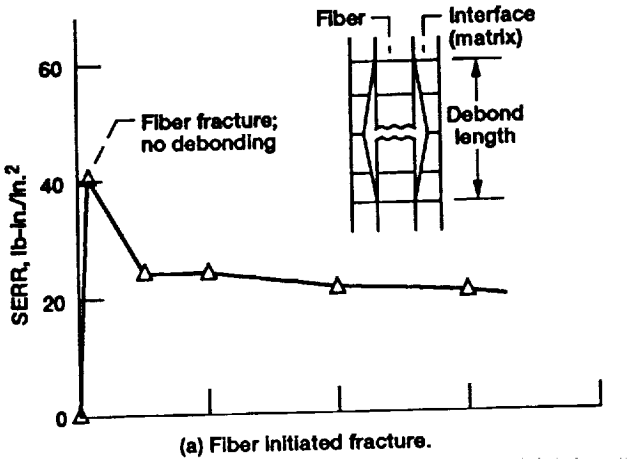

(a) Fiber initiated fracture.

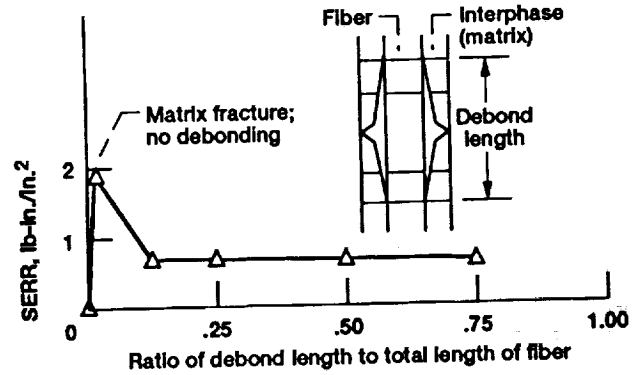

(b) Matrix initiated fracture.

Figure 1.—Strain energy release rate versus fiber debond length in a unidirectional composite under longitudinal load.

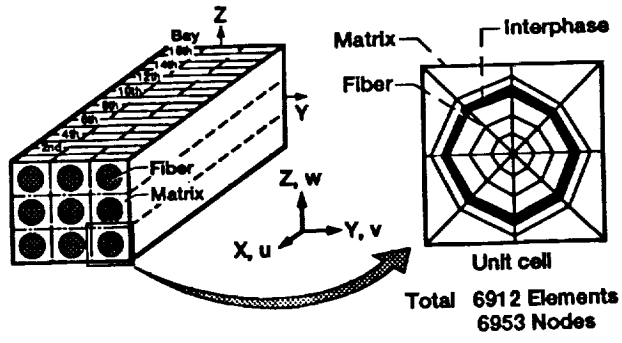

Figure 2.—Schematic diagram of unidirectional nine cell model.

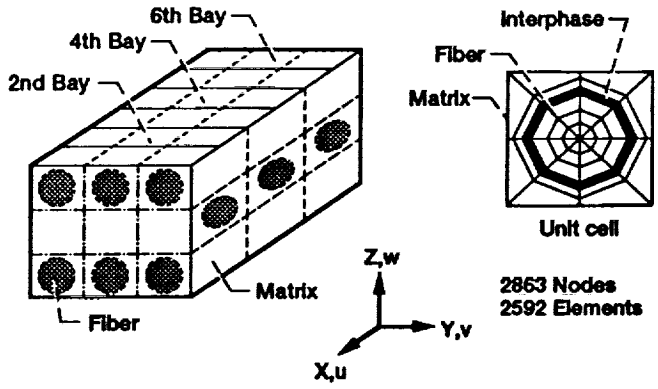

Figure 3.—Schematic diagram of crossply composite nine cell model.

$$\frac{P}{P_O} = \left[\frac{T_F - T}{T_F - T_O}\right]^n \left[\frac{S_F - \sigma}{S_F - \sigma_O}\right]^m \left[\frac{\dot{S}_F - \dot{\sigma}_O}{\dot{S}_F - \dot{\sigma}_O}\right]^\ell \left[\frac{\dot{T}_F - \dot{T}}{\dot{T}_F - \dot{T}_O}\right]^k \left[\frac{R_F - R}{R_F - R_O}\right]^p \cdots$$

$$\cdots \left[\frac{N_{MF} - N_M}{N_{MF} - N_{MO}}\right]^q \left[\frac{N_{TF} - N_R}{N_{TF} - N_{TO}}\right]^r \left[\frac{t_F - t}{t_F - t_O}\right]^s \cdots$$

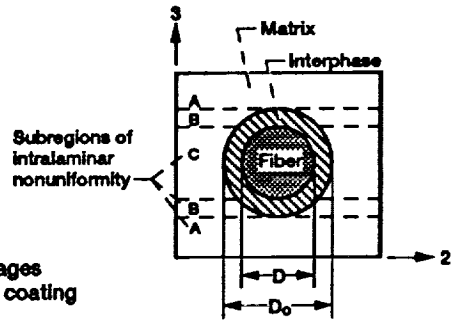

Rationale:

- Gradual effects during most range, rapidly degrading near final stages
- Representative of the in situ behavior for fiber, matrix, interphase, coating
- Introduction of primitive variables (PV)
- Consistent in situ representation of all constituent properties in terms of PV
- Room-temperature values for reference properties
- Continuous interphase growth
- Simultaneous interaction of all primitive variables
- Adaptability to new materials
- Amenable to verification inclusive of all properties
- Readily adaptable to incremental computational simulation

Notations:

P – property; T – temperature; S – strength; R – metallurgical reaction; N – number of cycles; t – time; over dot – rate; subscripts: O – reference; F – final; M – mechanical; T – thermal

Figure 4.—Assumed multifactor interaction relationship.

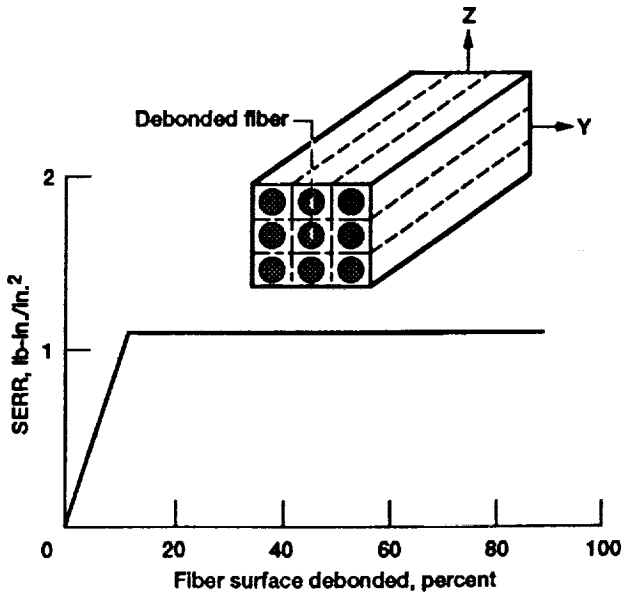

Figure 5.—Strain energy release rate for the unidirectional composite; cooling from 1500 °F to –300 °F; matrix initiated crack.

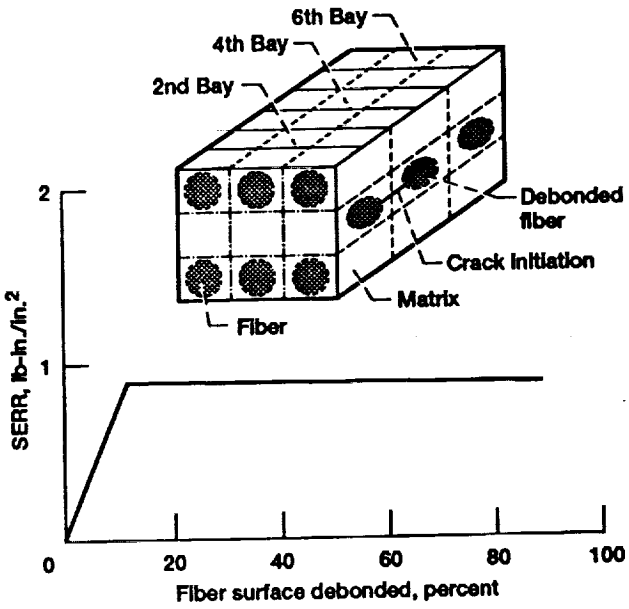

Figure 6.—Strain energy release rate versus fiber surface debonded for crossply composite, cooling from 1500 °F to –300 °F; intraply crack.

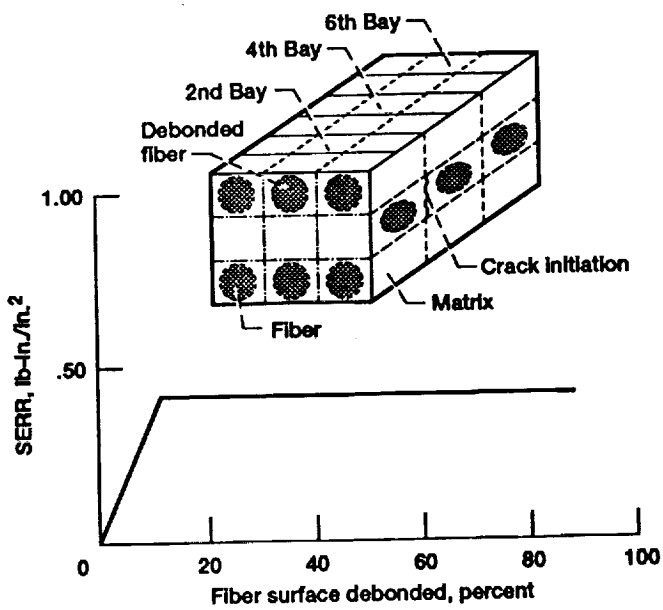

Figure 7.—Strain energy release rate versus fiber surface debonded; crossply composite under uniform cooling from 1500 °F to –300 °F; transply crack.

REPORT DOCUMENTATION PAGE

Form Approved
OMB No. 0704-0188

1. AGENCY USE ONLY (*Leave blank*)	2. REPORT DATE	3. REPORT TYPE AND DATES COVERED
	1991	Technical Memorandum

4. TITLE AND SUBTITLE

Thermally-Driven Microfracture in High Temperature Metal Matrix Composites

5. FUNDING NUMBERS

WU-510-01-0A

6. AUTHOR(S)

Subodh K. Mital and Christos C. Chamis

7. PERFORMING ORGANIZATION NAME(S) AND ADDRESS(ES)

National Aeronautics and Space Administration
Lewis Research Center
Cleveland, Ohio 44135-3191

8. PERFORMING ORGANIZATION REPORT NUMBER

E-6657

9. SPONSORING/MONITORING AGENCY NAMES(S) AND ADDRESS(ES)

National Aeronautics and Space Administration
Washington, D.C. 20546-0001

10. SPONSORING/MONITORING AGENCY REPORT NUMBER

NASA TM-105305

11. SUPPLEMENTARY NOTES

Prepared for the Symposium on the Mechanics of Composites at Elevated and Cryogenic Temperatures, ASME Applied Mechanics and Biomechanics Summer Conference, Columbus, Ohio, June 16-19, 1991. Subodh K. Mital, University of Toledo, Toledo, Ohio 43606 and NASA Resident Research Associate at Lewis Research Center. Christos C. Chamis, NASA Lewis Research Center. Responsible person, Subodh K. Mital, (216) 433-3261.

12a. DISTRIBUTION/AVAILABILITY STATEMENT

Unclassified - Unlimited
Subject Category 24

12b. DISTRIBUTION CODE

13. ABSTRACT (*Maximum 200 words*)

Microfracture (fiber/matrix fracture, interphase debonding and interply delamination) in high temperature metal matrix composites (HTMMC), subjected to thermal loading, is computationally simulated. Both unidirectional and crossply SiC/Ti15 composites are evaluated for microfracture driven by thermal loads, using multicell finite element models. Results indicate that under thermal loads alone, microfracture propagation is not as sensitive as it is under mechanical loads.

14. SUBJECT TERMS

Microfracture; Matrix fracture; Debonding; Metal matrix; Composites; Interface; Interphase; Thermal loads

15. NUMBER OF PAGES

12

16. PRICE CODE

A03

17. SECURITY CLASSIFICATION OF REPORT	18. SECURITY CLASSIFICATION OF THIS PAGE	19. SECURITY CLASSIFICATION OF ABSTRACT	20. LIMITATION OF ABSTRACT
Unclassified	Unclassified	Unclassified	